



# High-temperature conductivity evaluation of Nb doped SrTiO<sub>3</sub> thin films: Influence of strain and growth mechanism



Frédéric Aguesse <sup>a,b,\*</sup>, Anna-Karin Axelsson <sup>a</sup>, Patrick Reinhard <sup>c</sup>, Vasiliki Tileli <sup>a</sup>, Jennifer L.M. Rupp <sup>d</sup>, Neil McN Alford <sup>a</sup>

<sup>a</sup> Imperial College London, Department of Materials and London Centre for Nanotechnology, Exhibition Road, SW7 2AZ, London, UK

<sup>b</sup> CIC ENERGIGUNE, Parque Tecnológico de Alava, Albert Einstein 48, ED.CIC, 01510, Miñano, Spain

<sup>c</sup> Nonmetallic Inorganic Materials, ETH Zürich, Wolfgang-Pauli-Str. 10, HCI G539, CH-8093, Zürich, Switzerland

<sup>d</sup> Massachusetts Institute of Technology (MIT), Department of Materials Science and Engineering and Department of Nuclear Science and Engineering, Cambridge, MA 02139, USA

## ARTICLE INFO

### Article history:

Received 15 November 2012

Received in revised form 13 May 2013

Accepted 17 May 2013

Available online 24 May 2013

### Keywords:

Conductive oxides

Thin films

Induced strain

Doped perovskite

## ABSTRACT

Doped SrTiO<sub>3</sub> thin films, 55 nm thick, were epitaxially grown by Pulsed Laser Deposition with niobium contents ranging from 2 to 5 mol% on SrTiO<sub>3</sub> and LaAlO<sub>3</sub> substrates. The different templates result in different growth defects, film growth mechanism and therefore a different volume fraction of uniformly strained film under the critical thickness. The investigation of the conductivity reveals a significant difference between the two substrate choices, but only at elevated temperatures with conductivity values up to 30% larger for films on SrTiO<sub>3</sub> substrates compared with LaAlO<sub>3</sub>. Whereas in bulk ceramics the niobium level dictates the total conductivity, here it was found that the substrate choice had a greater influence for thin films, in particular at temperatures over 400 °C. This finding provides important information on conductive layers in complex heterostructures where strain and defects could work cooperatively.

© 2013 Elsevier B.V. All rights reserved.

## 1. Introduction

Highly conductive perovskite type thin films are attractive as bottom electrodes in heterostructures. Doped SrTiO<sub>3</sub> is an important candidate providing both high temperature stability and lattice compatibility with many functional materials. The electrical properties of SrTiO<sub>3</sub> can be tuned from insulating to semiconducting by intrinsic doping, through the control of the oxygen vacancy concentration in the perovskite structure, or by extrinsic doping, obtained from cation substitution producing either n- or p-type semiconducting behavior [1,2]. The most common n-type mechanism is typically achieved by substituting B site Ti<sup>4+</sup> by Nb<sup>5+</sup> [1,3–5] or A site Sr<sup>2+</sup> by La<sup>3+</sup> [1,2,6,7]. The extrinsic doping concentration level is usually proportional to the number of carriers present in the structure, which dictates the conductive and electric transport mechanism of the material. For bulk single crystals, niobium doped SrTiO<sub>3</sub> displays conductivity up to  $3.53 \times 10^{-4}$  S/m for a 4 mol% Nb doping (carrier concentration measured to  $3.3 \times 10^{20}$  cm<sup>-3</sup>) which reduces to  $9.5 \times 10^{-3}$  S/m for 2 mol% (carrier concentration measured  $1.6 \times 10^{20}$  cm<sup>-3</sup>) [6]. Commercial available SrTiO<sub>3</sub> based single crystals are grown by techniques at very high temperatures and expensive whereas nanostructured thin films would be a more cost-effective alternative for conductive layer or electrode structure.

In nanostructures, crystallographic arrangements and defects should be taken into account as films are often far from the ideal stoichiometry

when grown by energetic and vacuum deposition techniques, such as pulsed laser deposition (PLD), which introduce various extra defects such as oxygen deficiency. Moreover, when growing the film on a substrate, a compressive or tensile interfacial strain at the substrate-thin film interface may be formed. The impact of this interfacial strain on the ionic and electric conductivity of metal oxide materials has recently been reviewed [8] and originates from the local off-centering of the ions which affects the bond strength between the oxygen ion and the nearest neighbour cation, and changes the migration space of ions and electronic charge carriers [9–13]. However, there are limits to the volume of the film, where strain can be induced. Over a critical thickness the epitaxial film cannot maintain its strained structure and tends to release its energy by generating defects such as misfit dislocations, defects or island formation increasing the surface roughness. In addition, it is reported for the case of thin films that the conductivity has a strong dependence on the thickness increasing by four orders of magnitude for films of 45 to 300 nm thick [14]. Tomio et al. [15] investigated and compared Nb doped SrTiO<sub>3</sub> with undoped SrTiO<sub>3</sub> films grown by PLD and put forward a relation of the level of charge carriers formed, proposing a presence of Sr-cation vacancies, co-existence of Ti<sup>4+</sup>/Ti<sup>3+</sup>, Nb<sup>5+</sup> and oxygen vacancies in the Nb doped thin film. From above conclusions we find that there is no clear picture of how different growth templates affect the conductivity, particularly for elevated temperatures as conductivity for these type films are reported at room temperature or cryogenic temperatures.

It is obvious that the thin film processing history and resulting growth mode and structural order and disorder plays an important role in the

\* Corresponding author at: CIC ENERGIGUNE, Parque Tecnológico de Alava, Albert Einstein 48, ED.CIC, 01510, Miñano, Spain. Tel.: +34 622796354.

final result of conductivity. An example has been reported by Rupp [16], showing the relation between strain and ionic conductivity. The author revealed that lower total activation energy of conductivity was observed for an increase in strain in the case of ceria-based thin films.

Whereas the majority of reports have focused on room temperature and below for the conductivity evaluation, there are very few reports on doped  $\text{SrTiO}_3$  at elevated temperatures in air. The aim of this study is to investigate the influence of the substrate choice together with a series of niobium-doped levels (up to 5 mol%)  $\text{SrTiO}_3$  thin films on the conductivity in air at temperatures between 300 to 800 °C. Undoped  $\text{SrTiO}_3$  films could not be considered in the study as their resistivity is too high for these measurements. For the  $\text{SrTiO}_3$  substrates almost no strain is expected due to quasi identical lattice parameters between film and substrate whereas for  $\text{LaAlO}_3$  substrates with a lattice mismatch up to 3.3%, different interfacial strain is expected. The lattice strain from the growth template, as well as from the extrinsic doping of niobium were measured by X-ray diffraction and confirmed by transmission electron microscopy. The lattice evaluation compared with the measured conductivity will provide knowledge of the interplay of strain, film growth and electric conductivity for these heterolayer systems. The activation energy of total conductivity was evaluated along different temperature regions, shedding light on possible conduction mechanisms due to strain and defects.

## 2. Experimental part

### 2.1. Film processing, structural and microstructural analysis

Thin films of niobium doped  $\text{SrTiO}_3$  were grown by PLD on  $\text{LaAlO}_3$  (001) and  $\text{SrTiO}_3$  (001) single crystal substrates (SurfaceNet, Germany) from stoichiometric ceramic targets. Single phase and highly dense ceramic targets of  $\text{SrTi}_{1-x}\text{Nb}_x\text{O}_3$  were prepared by solid state chemistry with  $x = 0.020, 0.035$  and  $0.050$ . The unreacted powder was stoichiometrically mixed and calcined at 1100 °C, then pressed in a uniaxial press to a 20 mm diameter pellet followed by a sintering step at between 1360 and 1430 °C depending on amount of dopant. To ensure film reproducibility, the deposition conditions were kept identical between each deposition. Prior to the deposition, the substrates were cleaned with acetone, isopropanol, ultrapure water and nitrogen gas before mounting on the heated stage substrate holder inside the PLD chamber, and then gradually heated up to 700 °C inside the PLD chamber. An oxygen burn-off step ( $10^5$  Pa, 20 min) was then conducted to remove any residual organic materials on the surface of the substrate. The pressure of oxygen was set at 10 Pa during the deposition to compensate the typical oxygen loss occurring during PLD deposition but despite this oxygen atmosphere, a large number of vacancies is still expected in the film [17]. A KrF laser system was used to fire laser pulses at a frequency of 8 Hz forming a square-shape laser spot with a fluency of  $1.1 \text{ J.cm}^{-2}$  on the target enabling a slow film growth of  $0.4 \text{ \AA.s}^{-1}$  which facilitate the surface rearrangement and enable the system to reach a thermodynamic equilibrium. A thickness of 55 nm was kept identical between each film by using the same amount of pulses and the distance target to substrate fixed at 7.5 cm. After the deposition, the system was cooled down to room temperature at a rate of 10 °C/min to relax the lattice and interfaces.

The crystallographic orientation of the samples was determined by X-ray diffractometry (Philips X'pert Pro Diffractometer) using  $\text{Cu K}_\alpha$  radiation with monochromator and a nickel filter was added to remove the  $\text{K}_\beta$  wavelength. A high speed X'celerator detector was used to collect the data from 40 to 110°, which were processed using the X'pert HighScore Plus software. The Nelson Riley formula was used to evaluate the lattice parameters of the thin films [18]. Reciprocal space mapping was realised by tilting the sample by 45° in order to diffract the (220) planes of  $\text{LaAlO}_3$  and  $\text{SrTiO}_3$  substrates. Short  $2\theta - \omega$  scans were then performed at  $\Psi$  angles between 43 to 47° and the data were plotted using commercial data processing software after calculating the

reciprocal vector values. The surface of the sample was analysed using Atom Force Microscopy (AFM, Veeko Dimension) mounted with a silicon nitride cantilever.

For high resolution transmission electron microscopy (HRTEM) studies the films were prepared using an FEI Helios focused ion beam (FIB). To minimize the ion beam damage, low energy argon ions final thinning was performed at an accelerating voltage of 2 kV and a beam current of 28 pA, which prevent surface damage from the FIB preparation. HRTEM micrographs were acquired at 300 kV using a FEI Titan 80-300 equipped with a Cs corrector at the image plane.

### 2.2. Conductivity measurements

The conductive properties were measured with a high temperature dedicated measurement system by in-plane four point measurements in air. Electrodes of platinum strips of roughly 150 nm thickness were sputtered (SCD 050 Sputter Coater, Bal-Tec) through a stainless steel shadow mask. Platinum wires were then fixed to the sample with platinum paste (C 3605 P, Heraeus GmbH) and a two-component ceramic binder outside the film as more accurately described [19]. Electrical measurements were performed using a digital multimeter by DC four-point conductivity measurements (197 A, Keithley multimeter). The DC four point conductivity experiments were performed at a given single voltage of maximal 4 V across the thin film as a function of temperature in air. Measurements were done for 2 cycles between approximately 150 and 820 °C with heating and cooling rate of 3 °C/min and dwell time of 30 min. The first cooling curve was chosen for comparison between samples, since it is in thermal equilibrium upon cooling and no irreversible transformation was observed during the different thermal cycling.

## 3. Results and discussion

### 3.1. Microstructure and strain of Nb-SrTiO<sub>3</sub> films relative to substrate lattice misfit

The microstructures of the 3.5 mol% Nb doped  $\text{SrTiO}_3$  thin films prepared on  $\text{SrTiO}_3$  and  $\text{LaAlO}_3$  substrates were investigated by TEM and HRTEM. The structure of the two films is shown in Fig. 1a and e. The micrographs confirm the good reproducibility of the film thickness of 55 nm on the two different growth templates. In addition, a difference in texture aspect can clearly be observed between the two films. Fig. 1b and f depict close-ups of the films' regions. Both films exhibit regular damage caused by cross-sectional specimen preparation by focused ion beam which however has a minimum impact on the overall microstructure. When  $\text{SrTiO}_3$  serves as the template (no lattice mismatch with the film), the film grows uniformly on the substrate as evidenced by the minimum interfacial contrast (denoted by the white line in Fig. 1b). However, when  $\text{LaAlO}_3$  is used as the template high interfacial contrast exists. This indicates a high defect density at the substrate-film interface as can be noted in Fig. 1f. Planar defects propagate from the  $\text{LaAlO}_3/\text{Nb}-\text{SrTiO}_3$  interface to the top of the thin film in a kink band boundary aspect. Selected area electron diffraction (SAED) analysis (inset of Fig. 1e) of the film on the pseudo cubic  $\text{LaAlO}_3$  substrate shows diffraction spots splitting mainly along the out-of-plane direction. This is directly related to lattice distortion and strain due to the crystallographic incompatibility between the film and the substrate.

To clarify the origin of these defects, HRTEM images were acquired close to the interface of the two structures. Fig. 1c and d depict well the coherency of the lattice-matched  $\text{Nb}-\text{SrTiO}_3/\text{SrTiO}_3$  interface. This suggests a two dimensional (2D) nucleation process taking place throughout the 55 nm thick film. The strain associated energy seems to be relieved by local lattice distortions (black arrows in Fig. 1c and d). On the contrary, a high density of misfit dislocations is observed for the lattice-mismatched  $\text{Nb}-\text{SrTiO}_3/\text{LaAlO}_3$  interface (Fig. 1h and g). These misfit dislocations provide an incomplete strain relief for the film which further relaxes by producing stacking faults (Fig. 1h) or defect

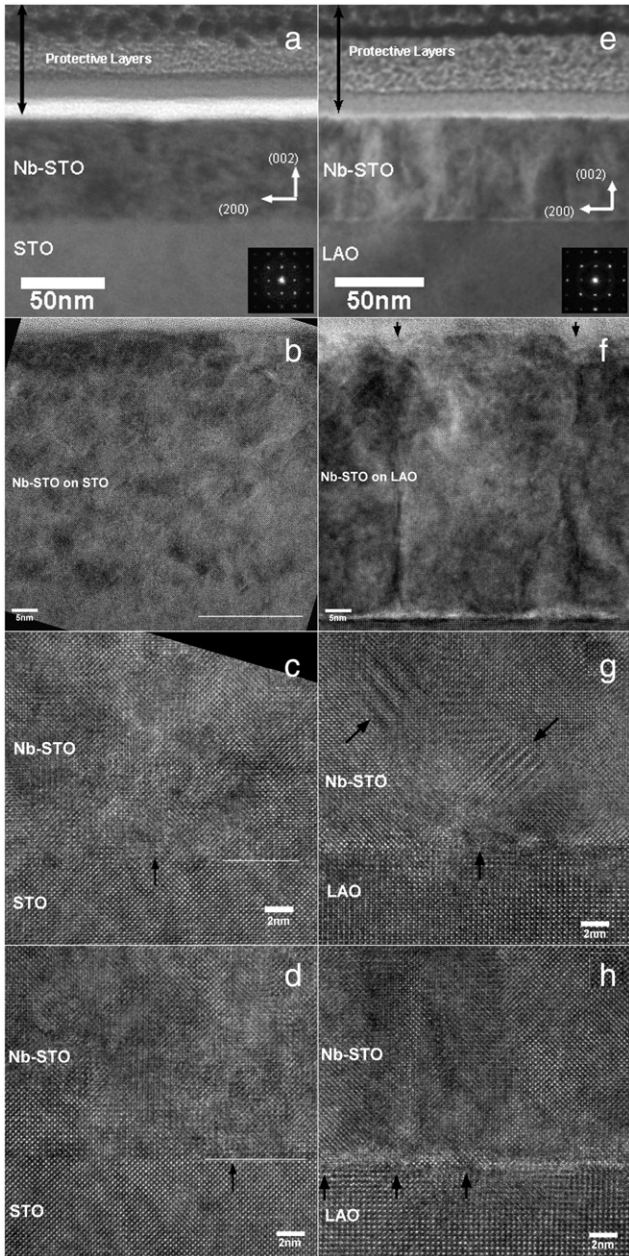


**Fig. 1.** Bright field transmission electron micrographs of cross sectional 3.5 mol% doped  $\text{SrTiO}_3$  thin film on  $\text{SrTiO}_3$  (a, b, c, d) and  $\text{LaAlO}_3$  (e, f, g, h) at increasing magnifications. SAED patterns of the two film structures are depicted as insets in (a) and (b). Black arrows in HRTEM images point to the interfacial distortions for the  $\text{Nb}-\text{SrTiO}_3/\text{SrTiO}_3$  structure (c and d) and the misfit dislocations leading to planar defects and stacking faults for the  $\text{Nb}-\text{SrTiO}_3/\text{LaAlO}_3$  heterostructure (g and h).

dislocation lines (Fig. 1g). Thus, a typical Stranski-Krastanov growth mode is very likely to occur for both film sets but with different strain releasing mechanisms. As a result, dissimilar lattice defects are associated with each and in the following we will probe electrical conduction properties of these two differently strained substrate-film sets. Moreover, the roughness of the thin film surface observed during the TEM analysis was confirmed by AFM measurements. Rougher surfaces with larger islands were observed on the films prepared on the  $\text{LaAlO}_3$  substrate compared to the surface of the films on  $\text{SrTiO}_3$  substrate. The surface of the thin films was confirmed by AFM as illustrated in Fig. 2a and b, representing the surface of the 5 mol% Nb doped  $\text{SrTiO}_3$  samples on  $\text{LaAlO}_3$  and  $\text{SrTiO}_3$ , respectively. The low root mean square (Rms) of the surface of these films indicates a low roughness of the sample and therefore low impact on the conductive properties are expected.

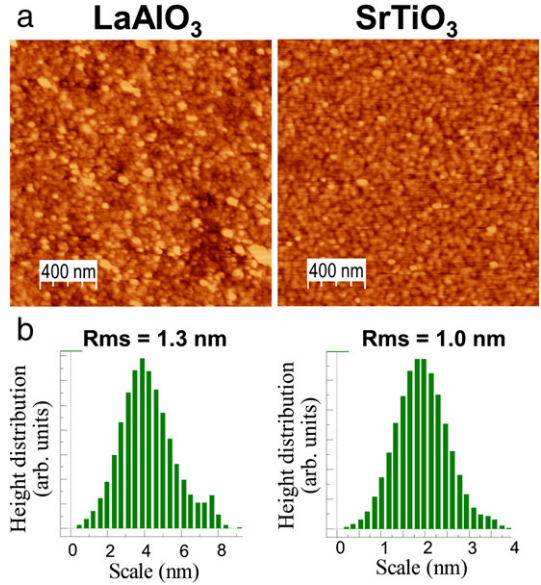


**Fig. 2.** (a) AFM images of 5 mol% Nb doped  $\text{SrTiO}_3$  thin films deposited on  $\text{LaAlO}_3$  and  $\text{SrTiO}_3$  substrate. (b) Percentage distribution of the height on the films surface as a function of the Z scale.

The XRD analysis of the samples (Fig. 3a and b) show sharp diffraction peaks belonging to the same family of planes ( $00\bar{1}$ ), indicating epitaxial growth in the out-of-plane direction. The same epitaxial growth is observed regardless the substrate and the dopant concentration.

Films on  $\text{SrTiO}_3$  substrate, Fig. 3b and inset, reveal peaks slightly separated from the substrate and clearly separated in the case of highest niobium dopant. This shift of the  $2\theta$  peaks indicates that despite a lattice mismatch  $< 0.2\%$ , the out-of-plane lattice parameter appears expanded.

For  $\text{LaAlO}_3$  substrates, where film peaks for all dopant levels are clearly visible, a shift towards lower  $2\theta$  values with increasing niobium dopant was seen, representing an increase in the  $c$ -direction by increasing the Nb content (seen in Fig. 3c). For identical 5 mol% Nb doped film on the two substrates, the shift of their respective  $2\theta$  values (002 peak) was greater for the films on  $\text{SrTiO}_3$  which would mean a smaller *in-plane* cell parameter in average (towards bulk values) when that substrate was used, if assuming a constant cell volume of the perovskite as also observed elsewhere by ref. [20].

Additional cell parameter and lattice information was obtained by reciprocal space mapping (RSM) around the scattering angles of the (220) diffracted planes of  $\text{SrTiO}_3$  and  $\text{LaAlO}_3$ . This measurement technique consists of successive  $2\theta$  XRD scans around a diffracted peak by varying the  $\psi$  angle by a step size of  $0.15^\circ$ . The measured distribution of intensity for 3.5 mol% doped films on  $\text{LaAlO}_3$  and  $\text{SrTiO}_3$  substrates seen in Fig. 4a and b, where the centre of the spot is inversely proportional to the lattice parameter.

In Fig. 4a, it can be observed that the spot originating from  $\text{Nb}-\text{SrTiO}_3$  signal is off-centred compare with the dotted red line, which serves as a visual guide line for the cubic structure position. This off-centring of the spot reveals that the film has lost its cubic symmetry towards a more distorted structure with  $a = b \neq c$ . From the RSM, an *in-plane* lattice constant of  $3.900 \text{ \AA}$  was determined for the 3.5 mol% doped thin film on  $\text{LaAlO}_3$  substrate which means a slight compression when compared with bulk, which confirms the increase of out of plane parameter evaluated from the  $2\theta$  XRD above.

For the same doped film but on  $\text{SrTiO}_3$ , the spot detection becomes harder due to the similar lattice parameters, but a higher resolution scan reveals a slight distortion not originating from the system distortion, which could further be identified via a  $2\theta$  scan at  $\psi = 44.47^\circ$ , shown as inset in Fig. 4b. This scan identifies the diffraction of (220) planes of  $\text{Nb}-\text{SrTiO}_3$  films separated from the substrate. The low intensity of the signal and the proximity with the substrate peak do not allow any

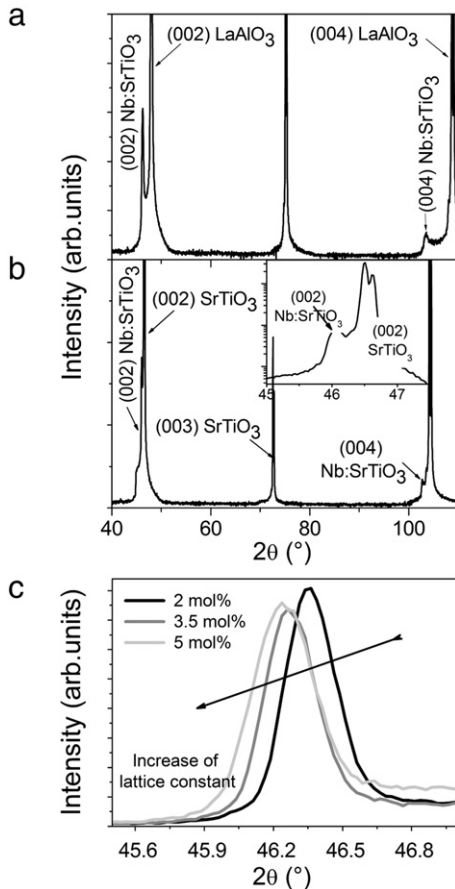


**Fig. 3.** XRD of 55 nm 5 mol% niobium doped SrTiO<sub>3</sub> film on LaAlO<sub>3</sub> (001) (a) and SrTiO<sub>3</sub> (001) (b) grown epitaxial in (001) direction. The inset in (b) focuses on the (002) peaks of film and substrate clarified by logarithmic scale. (c) Peak shift of the (002) diffracted plane with increasing niobium on LaAlO<sub>3</sub> substrate.

further identification of cell parameters but the observation of the lattice distortion reveals that the films on SrTiO<sub>3</sub> are also slightly compressed in-plane and expanded out-of-plane. The low lattice mismatch between Nb (3.5 mol%) doped SrTiO<sub>3</sub> and the SrTiO<sub>3</sub> substrate enables the film lattice to accommodate easily to the template in a cube-on-cube growth seen in the TEM diffraction pattern (SAED Fig. 1a) and this slight compression would produce few relaxional interfacial defects and an observed increase of the out-of-plane lattice parameters. A small compressive strain in-plane for similar films on SrTiO<sub>3</sub> substrate was previously reported by Ramadan et al. [14]. Furthermore, localized strain originating by the defects in a typical PLD film is known to be significantly larger than expected only by the unavoidable deviations in the stoichiometry [21].

The lattice parameters, where obtained, are compared with bulk lattice parameters as shown in Table 1. Due to resolution limitation, only comparison of the lattice constants of the films of 5 mol% Nb doped SrTiO<sub>3</sub> on both substrates is possible. This shows that the film deposited on LaAlO<sub>3</sub> possesses an out-of-plane lattice parameter of 3.925 Å, which is smaller than the film deposited on on SrTiO<sub>3</sub>, which is 3.944 Å, but both are larger than the bulk value of 3.9137 Å. This, as well as the RSM results, suggests a compressive in-plane strain. A previous report has also shown a compressive strain for niobium doped SrTiO<sub>3</sub> films on SrTiO<sub>3</sub> substrates [17]. The figure of merit for the strain out-of-plane can be calculated by:

$$\text{strain} = \frac{c_{\text{thin film}} - c_{\text{bulk}}}{c_{\text{bulk}}} \quad (1)$$

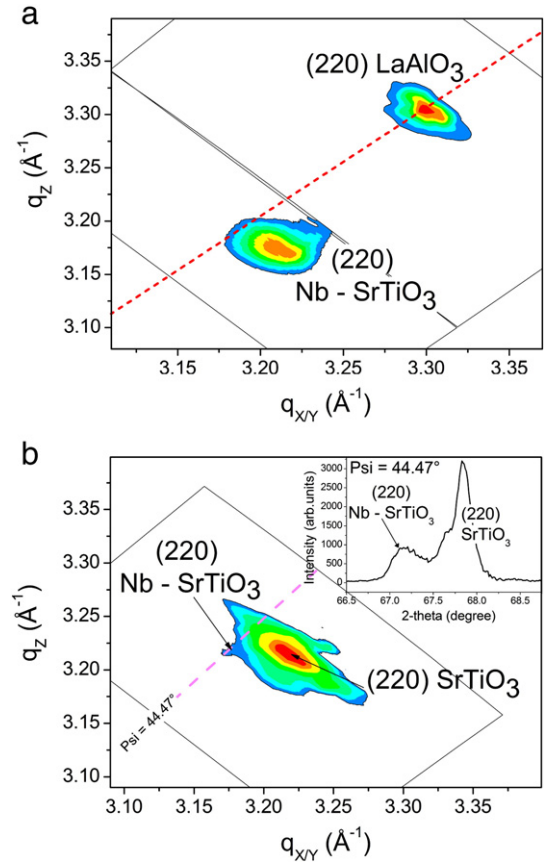


**Fig. 4.** Reciprocal space mapping of 3.5 mol% niobium doped SrTiO<sub>3</sub> (a) and SrTiO<sub>3</sub> (b) around the (220) diffracted peak of the substrates. The red line is a guide line for a cubic structure. The inset in (b) represents the 2θ scan measured along the pink dashed line at  $\psi = 44.47^\circ$ .

where  $c_{\text{thin film}}$  is the film lattice parameter in the out-of-plane direction and  $c_{\text{bulk}}$  represents the lattice parameter of the doped powder used as a target.

The two parameters affecting the lattice are: the insertion of niobium into SrTiO<sub>3</sub> lattice and the growth template which imposes a lattice mismatch. The increased cell volume with increasing niobium was attributed to the larger ionic radius of Nb<sup>5+</sup> (64 pm) substituting for Ti<sup>4+</sup> (60.5 pm) on the octahedrally coordinated B-site [1] and to the ionic repulsions around the formed cationic vacancies.

By comparing the 5 mol% Nb-doped film on LaAlO<sub>3</sub> and SrTiO<sub>3</sub> substrates, a lower out-of-plane lattice strain of +0.29% is found on LaAlO<sub>3</sub> (with a lattice mismatch of 3.29%) compared with SrTiO<sub>3</sub> of +0.77% (with a lattice mismatch of 0.3%).

In summary we have shown that a different growth mechanism is evident for films grown on different lattice matched substrates. Films grown on substrates with high lattice mismatch, such as LaAlO<sub>3</sub> produce defects in a close proximity to the interface, which propagates throughout the film to release the strain energy which further is accompanied by an island growth mode. Therefore a smaller out-of-plane strain compared with SrTiO<sub>3</sub> substrate was observed.

In contrast, films on SrTiO<sub>3</sub> exhibit a high volume fraction of coherent strain with a higher critical thickness before different relaxation mechanism appears. These different amounts and nature of defects can be used for enhancing the material performance where charge and ionic transport are possible along these defects. For the strained section, in particular in low doping concentrations as here, carrier mobility could be enhanced by the induced interatomic distances which may lower diffusion and transport energy barriers.

Table 1

Calculated lattice parameters and lattice strain of Nb-doped SrTiO<sub>3</sub> at various doping concentrations for 55 nm thick films. Calculations were conducted from the position of the observed (002) and (004) XRD peaks and using the Nelson Riley formula to eliminate the systematic errors.

	LaAlO <sub>3</sub>	SrTiO <sub>3</sub>	Nb (2 mol%) SrTiO <sub>3</sub>	Nb (3.5 mol%) SrTiO <sub>3</sub>	Nb (5 mol%) SrTiO <sub>3</sub>
Lattice parameters (bulk)	3.789 Å	3.905 Å	3.9054 Å*	3.9074 Å*	3.9137 Å*
film c-axis on LaAlO <sub>3</sub>	X	X	3.918 Å	3.924 Å	3.926 Å
lattice strain	X	X	+0.32% +/-0.03%	+0.42% +/-0.03%	+0.31% +/-0.03%
film c-axis on SrTiO <sub>3</sub>	X	X	—	—	3.9440 Å
Lattice strain	X	X	—	—	+0.77% +/-0.04%

\* Lattice parameters calculated by Rietveld refinement on powders before sintering the PLD targets.

### 3.2. Electric conductivity of Nb-doped SrTiO<sub>3</sub> thin films

The electrical conductivity of Nb-doped SrTiO<sub>3</sub> thin films was measured with respect to substrate (LaAlO<sub>3</sub> or SrTiO<sub>3</sub>) and extrinsic doping concentration for temperature ranging from 300 to 800 °C. In-plane DC electric measurements along the surface of the films have been carried out using a four-probe electrode geometry. This geometry allows us to separate voltage and current for resistance determination as detailed in Ref. [22].

Measurements over a range of temperature provides important information on the difference in conductivity from a thermodynamic point of view, where charge mobility resulting from defects, different thermal carrier excitations, impurities, strain can be addressed.

In Fig. 5a to c, the electrical conductivity is presented for the various doping level for films on both substrates; b and c are close ups for selected temperature of 650–800 °C. For all Nb-SrTiO<sub>3</sub> thin films electrical conductivity increases exponentially with increase in temperature. A classic semiconducting behaviour is observed due to increased thermal carriers' excitation with temperature (Fig. 5a). Nb-doped SrTiO<sub>3</sub> thin films exhibit a lower conductivity for deposition on LaAlO<sub>3</sub> substrate compared to the films on SrTiO<sub>3</sub> substrates, i.e. film conductivity is by 30% higher with 1600 S/m for depositions on SrTiO<sub>3</sub> relative to conductivity of 1140 S/m measured for LaAlO<sub>3</sub> substrates at 800 °C (Fig. 5b and c). Interestingly, the Nb-doping variation between 2 to 5 mol% does not affect conductivity despite the fact that microstructural evaluation revealed the insertion of niobium into the lattice. The contribution of the conductivity of the substrates was then evaluated by measuring bare substrates in identical conditions and their influence on the films conductivity was eliminated due to their low conductance.

Related conductivity evaluation was undertaken by Ramadan et al. [14] on LaAlO<sub>3</sub> and MgAl<sub>2</sub>O<sub>4</sub> and SrTiO<sub>3</sub> substrates finding that 300 nm films showed orders of magnitude increased electrical conductivity for the case of SrTiO<sub>3</sub>. The authors highlighted that in case of compressive strain as for deposition of Nb-doped SrTiO<sub>3</sub> on LaAlO<sub>3</sub>, Ti-O-Ti bonds of film locally tilt and electron orbital overlapping of Ti 3d-2t gets reduced. It is known from structural field maps relating orbital overlap and semiconducting properties in perovskites relative to cation size and their valence that this would lead to a reduction in electrical conductivity

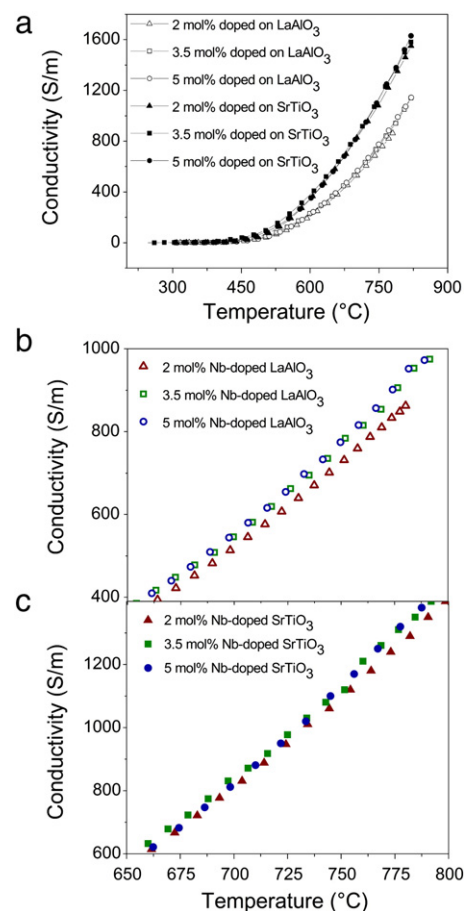


Fig. 5. (a) Temperature dependence of the electrical conductivity of Nb doped SrTiO<sub>3</sub> films for different niobium content and prepared on SrTiO<sub>3</sub> (001) and LaAlO<sub>3</sub> (001) substrates. Evolution of the conductivity between 660 °C and 800 °C for different Nb content films deposited on LaAlO<sub>3</sub> substrate (b) and SrTiO<sub>3</sub> substrate (c). The experimental error on the conductivity value is determined to be 1.8 % in this region of temperature.

[23]. It was also confirmed that these effects become strongest for small film thicknesses as strain per film volume increase. However, no structural proof of the hypothesis that for different growth and changes in associated defect densities per volume of film was given by authors and there was no study of activation energies of conductivity relative to film growth on different substrate materials. We observe that electrical conductivity is lower for case of Nb-doped SrTiO<sub>3</sub> on LaAlO<sub>3</sub> substrates due to a significant presence of film defects. The highest conductivities are observed for films deposited on SrTiO<sub>3</sub> substrates in this study. Interestingly, we observed lower conductivity for films deposited on LaAlO<sub>3</sub> substrates associated with an increased concentration of defect lines and stacking faults per film volume as detected by HRTEM (see Fig. 1e-h). The defects are observed to grow from the substrate to the air interface of the film in accordance to Stranski-Krastanov growth. Electrical conductivity is measured in-plane whereby charge carrier transport is lowered across these dislocation lines for the case of Nb-doped SrTiO<sub>3</sub> films on LaAlO<sub>3</sub> substrates. In the case of lowered concentration of defects per film volume, Nb-doped SrTiO<sub>3</sub> films on SrTiO<sub>3</sub> substrates, we observe an increased conductivity due to an easier conductivity path.

To estimate the conductivity thermodynamics, the activation energies of the total conductivity were extracted from the conductivity measurement using the modified Arrhenius formula, which enables to explicitly emphasize on the temperature dependence of the conductivity:

$$\sigma = \frac{\sigma_0}{T} \cdot \exp\left(\frac{-E_a}{RT}\right) \quad (2)$$

where  $\sigma$  is the conductivity,  $\sigma_0$  a constant pre-exponential factor and  $E_a$  the activation energy of the electrical conductivity

In Fig. 6 the activation energies for films with 5 mol% niobium doping on the two different substrates are shown exemplarily. All activation energy fits relative to temperature regions are summarized with respect to doping concentration of films and substrates in Table 2. For films on both substrates, it is obvious that a clear break of the Arrhenius slope can be observed at high temperature, revealing two different regions of activation energy. Whereas at lower temperature a third region can be assigned for films on SrTiO<sub>3</sub> substrate, a third region is not so obviously defined for films deposited on LaAlO<sub>3</sub>. The high resistivity of the films at these temperatures does not enable to clearly identify an Arrhenius slope break (Fig. 6). In accordance with observed lowered total conductivity for Nb-doped films on LaAlO<sub>3</sub> substrates high activation energies are observed in low temperature regime around 1.32 eV. At around 600 °C the activation energy reduces to 0.7 eV.

Under high defect concentration in the films, charge carriers move more slowly especially at low temperatures, resulting in an increase of

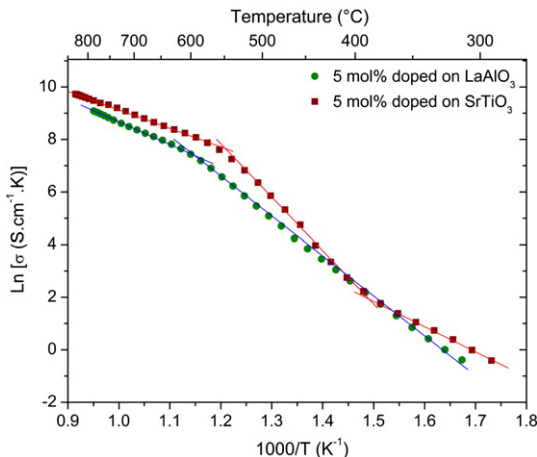


Fig. 6. Modified Arrhenius plot of total conductivity for 5 mol% Nb-doped SrTiO<sub>3</sub> thin films deposited on LaAlO<sub>3</sub> and SrTiO<sub>3</sub> substrates. The straight red lines are the fitting for activation energy calculation and used as eye guides.

Table 2

Activation energies total conductivity of Nb doped SrTiO<sub>3</sub> thin films deposited on LaAlO<sub>3</sub> and SrTiO<sub>3</sub> substrates for different level of niobium and at different range of temperature.

Activation energy for Nb-doped thin films					
On LaAlO <sub>3</sub> (eV)		On SrTiO <sub>3</sub> (eV)			
600 to 800 °C	300 to 555 °C	600 to 800 °C	415 to 555 °C	300 to 400 °C	
5 mol%	0.72 ± 0.06	1.31 ± 0.10	0.60 ± 0.06	1.63 ± 0.11	0.85 ± 0.10
3.5 mol%	0.68 ± 0.06	1.33 ± 0.11	0.63 ± 0.06	1.47 ± 0.10	0.95 ± 0.09
2 mol%	0.68 ± 0.06	1.32 ± 0.12	0.64 ± 0.06	1.38 ± 0.14	0.98 ± 0.12

the estimated activation energy. On SrTiO<sub>3</sub> substrates the activation energies of conductivity is lower with 0.9 eV that proved to have much less defect density than on LaAlO<sub>3</sub> which was observed by HRTEM. Also on SrTiO<sub>3</sub> substrate a beneficial strain under the critical thickness was observed. This strain may enable orbital overlapping plus less concentration of defects provides a better conduction path to the charge carriers. Apart from a high activation energy transition zone around 550 °C, films on SrTiO<sub>3</sub> show also a transition towards generally lower activation energy of 0.6 eV at 600 °C.

This clearly reveals a change of charge carriers relative to defect dislocation densities established through initial substrate choice in PLD processing and is in agreement with TEM observation.

Observation of a threshold temperature at which for both substrate types conductivity of films changes from high (low temperature) to low (high temperature) activation energy suggests a change in the dominant charge carriers in Nb-doped SrTiO<sub>3</sub> films. Sasaki, Maier and co-workers [24] have reported a similar trend for the case of Fe-doping in SrTiO<sub>3</sub> single crystals where they observed that at low temperature an increased activation energy was reported due to predominant ionic conductivity which changed to a predominant electronic conductivity at a threshold temperature around 500 °C. Even though electronic carriers (electrons instead of holes) may differ for given case of Nb-doping it is likely to attribute the observed high and low temperature activation energies for both substrates to a general change in the dominant carrier types. This general trend holds for all investigated samples whereby specific activation energies are affected by initial substrate and induced defect dislocation line densities in films for PLD growth.

Noteworthy, the impact of substrate choice and the resulting film defect and dislocation densities have a higher effect on the electrical conduction properties for these in-plane measurements rather than the effects of Nb-doping as initially expected. In Table 2, it can be seen that the activation energies show no variation with Nb doping and the variations are within the experimental error. However, solid solutions have clearly been formed in accordance with the XRD showing a unit cell variation. This is supported by previous observations [25,26] that undoped polycrystalline SrTiO<sub>3</sub> films exhibit higher activation energies around 1 eV for high temperature regime, and thus differ by 0.3–0.4 eV compared with these Nb-doped films.

From above measurement of microstructure related to conductivity evaluation, it can be concluded that defect dislocation lines which are perpendicular to the in-plane electrical conduction measurement direction retard the displacement of charge carriers and therefore lead to increased activation energies of conductivity. Since the films were grown epitaxial, one can relate the present findings to strain accommodation through substrate-film interface for film thickness at least up to 55 nm as presented here. In the case of low lattice misfit between film and substrate, smaller concentration of defect dislocation lines is formed and the motion of carriers is facilitated. This indicates that the impact of the substrate should be refrained on the thin film and suggests for applications that a large lattice mismatch between the deposited film and substrate is to be avoided to reduce the defect densities and facilitate carrier mobility in order to obtain better conductive properties.

#### 4. Conclusion

Thin films of niobium doped SrTiO<sub>3</sub> with doping level between 2 to 5 mol% were grown on single crystal LaAlO<sub>3</sub> and SrTiO<sub>3</sub> substrates. The crystallographic analysis comparing bulk and thin film lattice parameters confirmed complete solubility of the niobium dopant into the lattice. Depending on the lattice mismatch of film and substrate, the two different substrates resulted in different growth defects, film growth mechanism and therefore a different volume fraction of uniformed strained film under a critical thickness. From DC conductivity measurements a significant difference between the two substrate choices was observed when the samples were annealed up to 800 °C in air, but only at elevated temperatures with conductivity values up to 30% larger for films on SrTiO<sub>3</sub> substrates compared with LaAlO<sub>3</sub>. Here we compared equal thick films of 55 nm present a plausible reason for difference in conductivity over temperature.

The conductivity of the differently doped films grown on the different substrates was evaluated by the activation energy of total conductivity, where it was found that the degree of substitution did not vary the conductivity as much as the choice of substrate, unlike in reported bulk ceramics and single crystals where the niobium level dictates the total conductivity.

It was shown that the higher the volume fraction of the defect and film relaxation mechanisms, like found for films on LaAlO<sub>3</sub>, the more energy barriers exist for charge transfer and most likely alters the phonon vibrations negatively. The findings in this manuscript provide important information of conductive layers in complex heterostructures where strain and defects could work beneficial, in particular for stable high temperature electrodes.

#### Acknowledgements

The authors would like to acknowledge Dr Chin Phuah for TEM specimens preparation. F.A. was supported by EPSRC and J. L. M. R.

would like to acknowledge the Swiss National Science Foundation for the advanced researcher fellowship PA00P2-134153 for 2011/2012.

The I2CNER and International Research Center for Hydrogen Energy, Kyushu University Japan, is thanked for the visiting associate professorship in 2011/2012.

#### References

- [1] S. Ohta, T. Nomura, H. Ohta, M. Hirano, H. Hosono, K. Koumoto, 24th International Conference on Thermoelectrics, 168, 2005, p. 171.
- [2] D.P. Fagg, V.V. Kharton, A.V. Kovalevsky, A.P. Viskup, E.N. Naumovich, J.R. Frade, *J. Eur. Ceram. Soc.* 21 (2001) 1831.
- [3] O.N. Tufte, P.W. Chapman, *Phys. Rev.* 155 (1967) 796.
- [4] B. Gregory, J. Arthur, G. Seidel, *Phys. Rev. B* 19 (1979) 1039.
- [5] Q.-I. Zhou, *Europhys. Lett.* 71 (2005) 283.
- [6] S. Ohta, T. Nomura, H. Ohta, K. Koumoto, *J. Appl. Phys.* 97 (2005) 2108.
- [7] C.Q. Tang, Z. Xia, S. Yao, S. Chen, *Cryst. Res. Technol.* 31 (1996) 821.
- [8] J. Santiso, M. Burriel, *J. Solid State Electrochem.* 15 (2011) 985.
- [9] A. Kushima, B. Yıldız, *J. Mater. Chem.* 20 (2010) 4809.
- [10] A. Kushima, B. Yıldız, Y. Sindney, *Phys. Rev. B* 82 (2010) 115435.
- [11] W. Donner, C.L. Chen, M. Liu, J. Jacobsen, Y.-L. Lee, M. Gadre, D. Morgan, *Chem. Mater.* 23 (2011) 984.
- [12] J.A. Kilner, *Nat. Mater.* 7 (2008) 838.
- [13] I. Lubomirsky, *Monatsh. Chem.* 140 (2009) 1025.
- [14] W. Ramadan, S.B. Ogale, S. Dhar, S.X. Zhang, D.C. Kundaliya, I. Satoh, T. Venkatesan, *Appl. Phys. Lett.* 88 (2006) 2903.
- [15] T. Tomio, H. Miki, H. Tabata, T. Kawai, S. Kawai, *J. Appl. Phys.* 76 (1994) 5886.
- [16] J.L.M. Rupp, *Solid State Ionics* 207 (2012) 1.
- [17] K. Fukushima, S. Shibagaki, *Thin Solid Films* 315 (1998) 238.
- [18] P.E.Y. Flewitt, R.K. Wild, in: B. Cantor, M.J. Goringe (Eds.), *Physical Methods for Material Characterization*, Institute of Physics Publishing, Philadelphia, 1994, p. p517.
- [19] J.L.M. Rupp, L.J. Gauckler, *Solid State Ionics* 177 (2006) 2513.
- [20] Y.L. Zhu, X.L. Ma, D.X. Li, H.B. Lu, Z.H. Chen, G.Z. Yang, *Acta Mater.* 53 (2005) 1277.
- [21] M. Brooks, L.F. Kourkoutis, T. Heeg, J. Schubert, D.A. Muller, D.G. Schlom, *Appl. Phys. Lett.* 94 (2009) 162905.
- [22] P.J. Gellings, H.J.M. Bouwmeester, *Handbook of Solid State Electrochemistry*, CRC Press, 1997. 163 , (chapter 5 (Defect Chemistry in Solid State Electrochemistry)).
- [23] K. Kamata, T. Nakamura, T. Sata, *Bull. Tokyo Inst. Technol.* 120 (1974) 73.
- [24] K. Sasaki, J. Claus, J. Maier, *Solid State Ionics* 121 (1999) 51.
- [25] N.H. Chan, R.K. Sharma, D.M. Smyth, *J. Electrochem. Soc.* 128 (1981) 1762.
- [26] S.H. Kim, J.H. Moon, J.H. Park, J.G. Park, Y. Kim, *J. Mater. Res.* 16 (2001) 192.